Elastic and viscous properties of the nematic dimer CB7CB

Greta Babakhanova, Zeinab Parsouzi, Sathyanarayana Paladugu, Hao Wang, Yu. A. Nastishin, Sergij V. Shiyanovskii, Samuel Sprunt, and Oleg D. Lavrentovich

Phys. Rev. E **96**, 062704 — Published 26 December 2017

DOI: 10.1103/PhysRevE.96.062704

Elastic and viscous properties of nematic dimer CB7CB

Greta Babakhanova,[1,2] Zeinab Parsouzi,[3] Sathyanarayana Paladugu,[1] Hao Wang,[1,2] Yu. A. Nastishin,[1,4] Sergij V. Shiyanovskii,[1] Samuel Sprunt,[3†] and Oleg D. Lavrentovich[1,2,3*]

[1]*Liquid Crystal Institute, Kent State University, Kent, OH 44242, USA.*

[2]*Chemical Physics Interdisciplinary Program, Kent State University, Kent, OH 44242, USA.*

[3]*Department of Physics, Kent State University, Kent, OH 44242, USA.*

[4]*Hetman Petro Sahaidachnyi National Army Academy, 32, Heroes of Maidan St., Lviv 79012, Ukraine*

Abstract

We present a comprehensive set of measurements of optical, dielectric, diamagnetic, elastic and viscous properties in the nematic (N) phase formed by a liquid crystalline dimer. The studied dimer, 1,7-bis-4-(4′-cyanobiphenyl) heptane (CB7CB), is composed of two rigid rod-like cyanobiphenyl segments connected by a flexible aliphatic link with seven methyl groups. CB7CB and other nematic dimers are of interest due to their tendency to adopt bent configurations and to form two states possessing a modulated nematic director structure, namely, the twist bend nematic, $N_{TB,}$ and the oblique helicoidal cholesteric, Ch_{OH}, which occurs when the achiral dimer is doped with a chiral additive and exposed to an external electric or magnetic field. We characterize the material parameters as functions of temperature in the entire temperature range of the N phase, including the pre-transitional regions near the N-N_{TB} and N-to-isotropic (I) transitions. The splay constant K_{11} is determined by two direct and independent techniques, namely, detection of the Frederiks transition and measurement of director fluctuation amplitudes by dynamic light scattering (DLS). The bend K_{33} and twist K_{22} constants are measured by DLS. K_{33} being the smallest of the three constants, shows a strong non-monotonous temperature dependence with a negative slope in both N-I and N-N_{TB} pretransitional regions. The measured ratio K_{11} / K_{22} is larger than 2 in the entire nematic temperature range. The orientational viscosities

† ssprunt@kent.edu

* Corresponding author: olavrent@kent.edu

associated with splay, twist and bend fluctuations in the N phase are comparable to those of nematics formed by rod-like molecules. All three show strong temperature dependence, increasing sharply near the N – N_{TB} transition.

I. INTRODUCTION

Liquid crystals spectacularly illustrate how subtle variation in molecular structure leads to dramatic changes in the macroscopic properties of a material. Rigid rod-like molecules such as 4′-pentyl-4-cyanobiphenyl (5CB) are known to form the nematic (N) phase with a long range orientational order and no positional order; in the N phase, the rod-like molecules are on average aligned along a single direction, specified by a unit vector $\hat{\mathbf{n}}$ called the director. However, when two cyanobiphenyl moieties are linked into a single molecule by a flexible aliphatic chain with an odd number of methyl groups, as in the case of 1,7-bis-4-(4′-cyanobiphenyl) heptane (CB7CB), a new, lower temperature nematic phase, the so-called twist-bend nematic (N_{TB}), emerges [1-3]. This phase exhibits a uniform mass density but a spatially modulated and locally chiral director field. The director precesses helically on a cone with an extremely small period (pitch), measured by transmission electron microscopy (TEM) [2,3] to be about 8 nm. The nanoscale heliconical geometry is evidenced by characteristic textures of asymmetric Bouligand arches in freeze-fracture TEM observations [3] and by resonant X-ray scattering [4].

The heliconical structure of the N_{TB} phase, which was theoretically predicted by Meyer [5], Dozov [6] and Memmer [7], is a result of the tendency of molecules to adopt spontaneous bent conformations; the twist is required to yield a spatially uniform bend. In Dozov's theory, the transition from the N to N_{TB} is associated with a change of the sign of the bend elastic constant K_{33} from positive to negative. A periodically modulated N phase of an alternative splay-bend type can also be realized as a combination of periodic bend and splay [5,6]. The relative stability is controlled by the ratio of the splay K_{11} to twist K_{22} elastic constants; the N_{TB} variant is stable when $\frac{K_{11}}{K_{22}} > 2$ [6].

The dimer material CB7CB, in addition to N_{TB}, also exhibits another twist-bend structure, the so-called oblique helicoidal cholesteric, Ch_{OH}, when doped with a small amount of chiral additive and subjected to an externally applied electric [8,9] or magnetic [10] field. Here again,

the experimental observations followed earlier theoretical predictions by Meyer [11] and de Gennes [12]. In an ordinary cholesteric, the molecules twist in a helical fashion with the director remaining perpendicular to the helical axis. In the Ch_{OH} structure, the director twists while making an angle $\theta < \pi / 2$ with the twist axis and the direction of the applied field. The tilt introduces bend in addition to twist. However, when the bend elastic constant is small, the elastic energy penalty for bend is compensated by the dielectric energy gain associated with the nonzero projection of the local director on the field direction. Geometrically, the director structure of the Ch_{OH} is similar to that of the N_{TB} phase, but the pitch P of the Ch_{OH} is typically much larger than the nano-scale pitch of the N_{TB}, since the molecules in the Ch_{OH} can rotate around their long axes [13], while the local structure of N_{TB} inhibits this rotation and is essentially biaxial. Both θ and P in Ch_{OH} are explicit functions of the applied field and the ratio $\frac{K_{33}}{K_{22}}$ [8,11]. The sensitivity of the pitch to the electric field makes it possible to realize electrically controlled selective reflection of light [9] and lasing [14] within broad spectral ranges, which are potentially useful effects for practical applications of Ch_{OH}. The important parameter to optimize in these applications is the ratio $\frac{K_{33}}{K_{22}}$, which depend on temperature. Measurements such as those reported here are crucial to explore the potential for this optimization.

The sensitivity of both N_{TB} and Ch_{OH} to the elastic constants of the corresponding material in its N state motivate the work reported here. In particular, we experimentally determine the temperature dependence of all three bulk elastic constants in the entire range of the nematic phase of the dimer CB7CB. These three constants are deduced from the dynamic light scattering (DLS) data and also, in the case of splay constant, from the Frederiks transition threshold in the electric field. The elastic properties of CB7CB have been explored in the past [15-19], but the data obtained by different groups differ from each other rather substantially.

To date, the most complete study has been presented by Yun et al [15] who determined the temperature dependencies of all three bulk elastic constants by an electro-optical technique. Yun et al [15] used a Frederiks transition in a planar cell to determine the splay elastic constant K_{11} from the threshold of director deformations caused by an applied electric field. As the field increases, the initial pure splay mode of deformations is replaced by a mixed splay-bend distortion. By fitting the capacitance response of the cell with an analytical expression in which the elastic

parameter is of the form $\kappa = (K_{33} - K_{11})/K_{11}$, one can extract the value of K_{33} since K_{11} is known. The method has been originally proposed for nematics formed by rod-like molecules [20], in which K_{33} is significantly larger than K_{11}, so that the fitting parameter κ is large and the fitting of extrapolated response is robust. In the case of dimers, however, it is expected that the largest elastic constant is K_{11} while K_{33} is the smallest [1,21-23]. Therefore, the low energy cost of bend distortions and small contribution of K_{33} to the fitting parameter κ makes the extrapolation approach less robust for the dimers. The ratio $\frac{K_{11}}{K_{22}}$ was found to be around 1.4, i.e., smaller than 2, near the N- N_{TB} phase transition [15]. The result is somewhat surprising, since the inequality $\frac{K_{11}}{K_{22}} > 2$ represents a criterion of the formation of the N_{TB} phase as opposed to a splay-bend phase. The very fact of the twist-bend deformations in the low-temperature nematic phase has been established in the case of CB7CB by the freeze-fracture transmission microscopy studies [3] and by the resonant carbon soft X-ray scattering [4]. Sebastian et al and Lopez et al [16,19] used the same extrapolation technique of splay Frederiks transition to determine K_{11} and K_{33}; it was found that as the temperature decreases towards the N-N_{TB} transition, K_{11} monotonously increases while K_{33} first increases and then decreases. The values of K_{11} determined in [16,19] were somewhat higher (by $\approx$ 4-5%) than those in Ref. [15], while the values of K_{33} in [16,19] were higher than those in Ref. [15] by approximately a factor of 2, depending on the temperature.

Qualitatively different results were presented by Parthasarathi et al [18] who reported that as the temperature is lowered towards the N-N_{TB} transition in pure CB7CB, the bend constant K_{33} increases rather than decreases. Therefore, the prior experimental results on the elastic constants of the nematic phase of CB7CB are rather controversial. In light of the importance of this material for understanding of N_{TB} and Ch_{OH} structures, the issue needs to be revisited.

In this work, we use direct and complementary techniques to determine all three elastic constants of CB7CB as well as other material parameters. The electro-optic version of the Frederiks effect is used only to find the splay elastic constant K_{11} from the direct measurements of the threshold voltage needed to cause director distortions. To find the bend and twist constants and to independently determine the splay constant, we use dynamic light scattering (DLS). The

two independently determined values of K_{11} served as a test of reliability. Light is scattered at fluctuations of the director which is the local optic axis of the nematic. By designing a proper geometry of the experiment (polarizations, incident and scattering angles), one can separate contributions of different modes of deformations and, in particular, probe the deformations of pure bend. As we demonstrate in this paper, this extraction of bend is especially well suited for the dimeric materials in which K_{33} is the smallest of all three bulk constants. Furthermore, besides the direct information about the elastic properties, the DLS data, with a proper calibration, also yield the values of orientational viscosities, corresponding to the relaxation dynamics of splay, bend, and the predominantly twist component of twist-bend deformations, as described by Majumdar et al [24] and Zhou et al [25]; these viscosities are presented as functions of temperature. Finally, this work presents results on other material properties of CB7CB, including refractive indices, birefringence, dielectric permittivities and diamagnetic anisotropy. The results are of importance in deepening our understanding of the material properties leading to the N_{TB} and Ch_{OH} twist-bend states and in optimization of electrically tunable selective reflection of light and lasing utilizing the Ch_{OH} structure.

II. EXPERIMENTAL DETAILS

A. Chemical structure, phase diagram, and alignment

The chemical structure and the phase diagram of CB7CB are shown in Fig. 1. Phase characterization was performed upon cooling with the rate of $0.1\,^{\circ}/\mathrm{min}$ using polarizing optical microscopy (POM). The temperature was controlled with an Instec HCS402 hot stage and mK2000 temperature controller with a temperature stability of $0.01\,^{\circ}\mathrm{C}$. The CB7CB was synthesized following the procedures reported by Chen et al [2]. Planar alignment was promoted by spin-coating PI2555 (HD Microsystems) polyimide layer on indium tin oxide (ITO)-coated glass substrates. The uniform alignment was achieved by rubbing the substrates with a velvet cloth. The cells were assembled with anti-parallel arrangement of the rubbing direction. The cell gap d was controlled by Micropearl glass spacers (mixed with NOA 71 UV glue), and measured using a Perkin Elmer UV/VIS Spectrometer Lambda 18. All the experimental cells were filled by capillary

action in the I phase. Figure 2 shows the POM textures of the N and N_{TB} phases in a planar cell ($d = 18.9\ \mu\text{m}$).

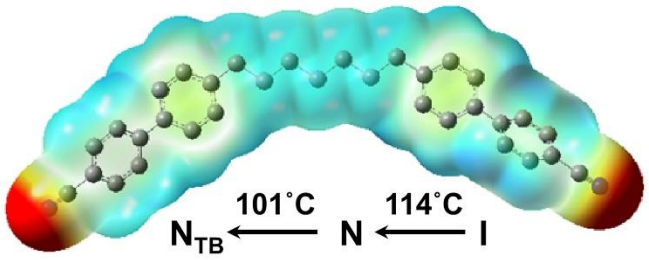

FIG 1. (Color online) Molecular structure of CB7CB with electrostatic potential surface and phase diagram upon cooling (negative and positive electric charges excesses are shown as red and blue, respectively).

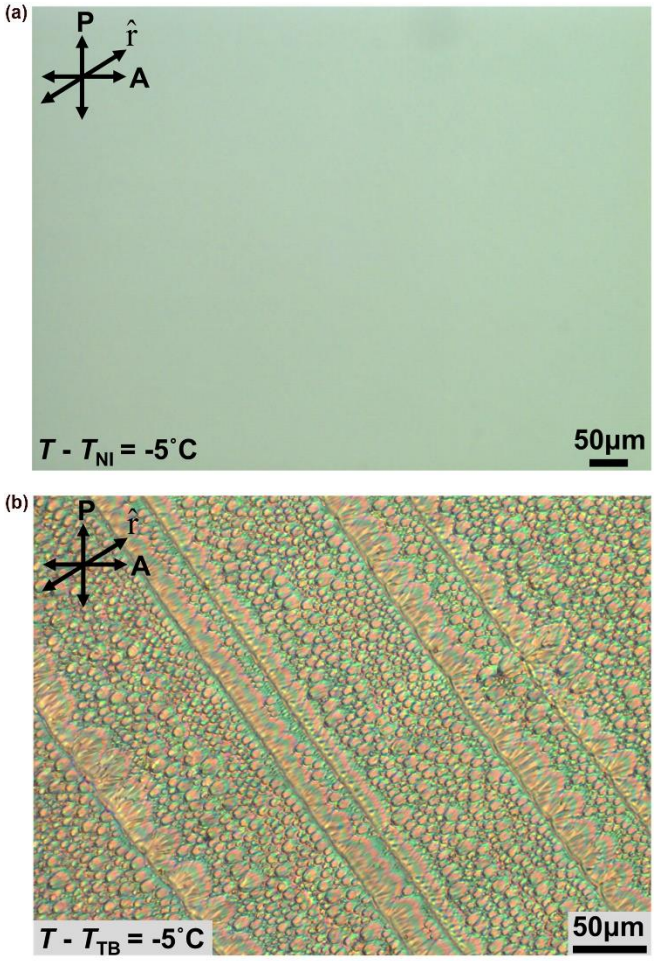

FIG 2. (Color online) POM textures of CB7CB under cross polarizers showing uniformly aligned (a) N and (b) N_{TB} phases with focal conic domains. The direction of rubbing is shown by the axis $\hat{\mathrm{r}}$.

B. Refractive indices and birefringence

We used the wedge-cell technique [26] to determine the ordinary n_o and extraordinary n_e refractive indices of CB7CB. The wedge cell was prepared using planar, rubbed ITO substrates assembled in antiparallel fashion such that the rubbing direction was perpendicular to the wedge thickness gradient. The pretilt angle in the planar substrates measured using crystal rotation method [27] is less than $1°$. The thickness of the thick part of the wedge was set by a stripe of NOA 71 glue with pre-mixed Micropearl glass spacers. Initially, the optical interference technique described in [26] was used to determine the angle of an empty wedge, by shining a Helium-Neon (He-Ne) laser beam ($\lambda = 633$ nm) onto the cell and recording an interference pattern under the POM. The temperature dependence of the wedge angle was determined over the same temperature range as the nematic range. The wedge cell was then filled with CB7CB by capillary action in the I phase. The analyzer (A) and polarizer (P) were aligned parallel to each other. Their orientations with respect to the nematic director were chosen to explore n_o and n_e independently. When polarization directions of both A and P are perpendicular or parallel to $\hat{\mathbf{n}}$, the multiple-beam interference in the wedge cell yielded n_o or n_e, respectively, according to the following equation

$$n_{o,e} = \frac{l\lambda}{2\alpha(s_{m+l}^{o,e} - s_m^{o,e})}, \tag{1}$$

where l is the interference order (i.e. the fringe number), λ is the wavelength of probing light, α is the wedge angle, and $(s_{m+l}^{o,e} - s_m^{o,e})$ is the distance between the interference maxima [26].

The Senarmont technique was employed to verify the birefringence, Δn, due to the higher sensitivity of this method [28]. The experimental optical set-up is displayed in Fig. 3. First, a polarizer and analyzer (positioned on motorized rotational stage), were crossed for maximum extinction. A quarter-wave plate was placed such that the optical axis is parallel to the initial polarizer. The planar cell ($d = 10.1\ \mu$m) was introduced with the rubbing direction, $\hat{\mathbf{r}}$, making an

angle $\varphi_o = 45°$ with the fist polarizer. The sample was probed with He-Ne laser light. For each temperature scan, the analyzer was rotated until the intensity of the linearly polarized light emerging from the quarter-wave plate reached a minimum ($I_{\min}$) corresponding to an angle β. The maximum error of the angle measurements was $1°$. The total phase retardation was calculated as $\Delta\Phi = 2\beta + N2\pi$, where N is an integer number, and the resultant birefringence is determined as

$$\Delta n = \frac{\lambda}{2\pi d}\Delta\Phi \tag{2}$$

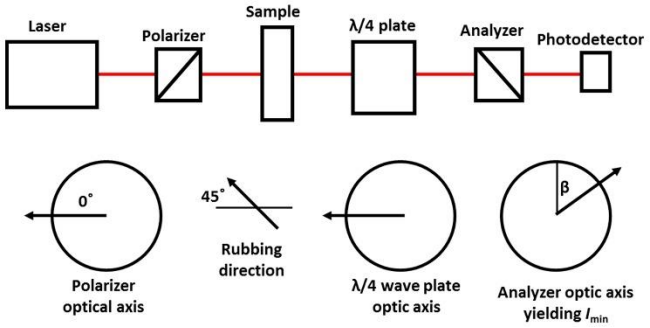

FIG 3. (Color online) Senarmont experimental set-up for birefringence measurements**.**

To diminish the contribution from experimental errors, we fitted the measured Δn and $(n_e + n_o)$ data with a polynomial fit and obtained smoothed data for the temperature dependence for the refractive indices, according to the equation:

$$n_{e,o} = \frac{(n_e + n_o) \pm (n_e - n_o)}{2} \tag{3}$$

C. Electro-optical measurements

Dielectric characterization was performed using a precision LCR meter 4284A (Hewlett Packard). Temperature-dependent dielectric permittivities were calculated from the capacitance measurements on a planar cell ($d = 18.9\ \mu$m) of CB7CB. A voltage (V) up to 20 V_{rms} was applied across the active area of the patterned ITO electrodes. The square ITO patterned area was 25 mm^2. The measurements were performed at frequencies: $f = 5, 10, 20, 40$ and 60 kHz. No significant

dissipation was observed in the range 5-200 kHz. The perpendicular component of dielectric permittivity $\varepsilon_{\perp}$ was calculated from capacitance measurements at low voltages, below the Frederiks threshold, whereas the parallel component $\varepsilon_{\parallel}$ was determined by extrapolation method at high voltages. The cell capacitance C was plotted as a function of V to find the splay Frederiks threshold voltage (V_{th}) by the double-line extrapolation method. The splay elastic constant K_{11} was then calculated according to

$$K_{11} = \frac{\varepsilon_{\text{o}} \Delta\varepsilon V_{\text{th}}^2}{\pi^2}, \tag{4}$$

where $\Delta\varepsilon = \varepsilon_{\parallel} - \varepsilon_{\perp}$ and $\varepsilon_{\mathbf{o}}$ is the vacuum permittivity.

D. Diamagnetic anisotropy

The diamagnetic anisotropy, $\Delta\chi$, was determined utilizing a planar cell ($d = 18.9\ \mu\text{m}$) placed in a uniform magnetic field applied perpendicular to the bounding plates (Fig. 4). The sample was positioned between two crossed polarizers with the rubbing direction $\hat{\mathbf{r}}$ making an angle of $45°$ with the polarizer axes. The director reorientation caused by the splay Frederiks transition was monitored via transmitted light intensity data. Subsequently, the magnetic threshold (B_{th}) was extrapolated from measurements of the optical phase retardance vs. magnetic field curve using a double-line extrapolation approach. The values of $\Delta\chi$ were calculated by relating electric and magnetic splay Frederiks effects according to

$$\Delta\chi = \varepsilon_{\text{o}} \mu_{\text{o}} \Delta\varepsilon \left(\frac{V_{\text{th}}}{dB_{\text{th}}} \right)^2 \tag{5}$$

where $\mu_{\text{o}} = 4\pi \times 10^{-7}$ H/m is the vacuum permeability.

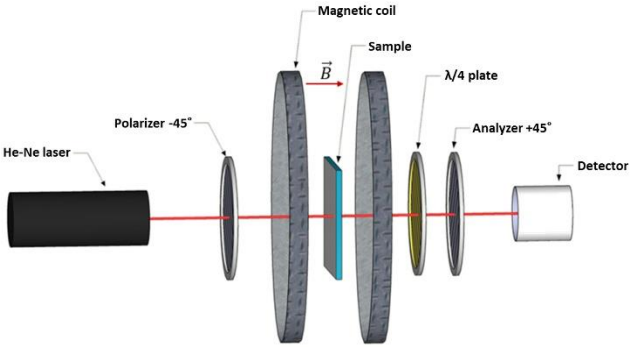

FIG 4. (Color online) Optical set-up to determine $\Delta\chi$.

E. Dynamic light scattering

Dynamic light scattering (DLS) on planar cells ($d = 16.5\ \mu$m) of CB7CB was conducted as a function of temperature on cooling. In order to obtain the absolute values of K_{11}, K_{22} and K_{33}, we additionally recorded light scattering from a sample of the well-characterized calamitic nematic 4-*n*-octyloxy-4*'*-cyanobiphenyl (8OCB), for which the elastic constants and refractive indices are known with high precision [29-31]. The 8OCB experiments were performed at selected temperatures and under the same experimental conditions as for CB7CB, using a planar cell ($d = 14.4\ \mu$m). Specifically, 8OCB and CB7CB cells were situated in the same plane and placed adjacent to each other in the scattering apparatus. They could then be translated into or out of the incident laser beam by turning a single micrometer, with no other effect on the state or parameters of the experiment. High quality of homogeneous $\hat{\mathrm{n}}$ alignment was confirmed by POM, performed in situ on the DLS set-up. Phase transition temperatures of test samples were checked both before and after the experiment.

In the light scattering set-up, the output of a He-Ne laser (Spectra-Physics, model 127), with a wavelength $\lambda_o = 633$ nm, incident power of 4 mW, and polarization oriented perpendicular to the scattering plane, is focused onto a spot on the sample with diameter ~50 μm. The hot stage containing the control and test samples was installed on a three-stage goniometer that allowed independent adjustment of the incident angle (set to normal incidence), the scattering angle, and the angle of the director $\hat{\mathbf{n}}$ with respect to the scattering plane. This flexibility enabled us to isolate scattering from three components of the director fluctuations: pure bend (K_{33}), twist-bend mode

dominated by twist (K_{22}), and pure splay (K_{11}) (Fig.5). In each case, depolarized scattered light was collected through a pinhole-lens-optical fiber detection layout. Scattered photons were converted to electronic pulses through a photomultiplier-amplifier-discriminator combination, allowing homodyne time correlation functions of the scattered intensity to be computed on a digital correlator.

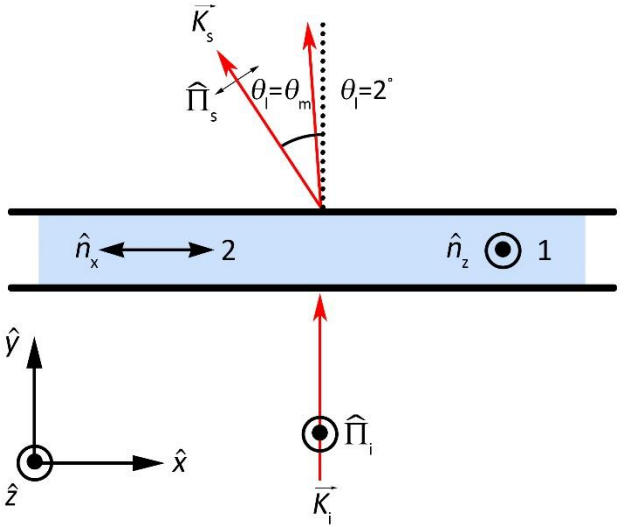

FIG 5. (Color online) Light scattering geometries. "1": splay+twist scattering; "2": pure bend scattering ($\theta_l = \theta_m$) and predominantly twist scattering ($\theta_l = 2°$). $\vec{K}_i$ and $\vec{K}_s$ correspond to incident and scattering wave vectors respectively; θ_l is scattering angle measured in the laboratory frame; θ_m refers to the so-called "magic angle"; Π_i and Π_s indicate the light of incident polarization and scattering polarizations which are orthogonal to each other.

In splay+twist geometry "1" of Fig. 5, the scattering vector $\vec{q}$ representing the difference between the incident and scattered wave-vectors, $\vec{q} = \vec{K}_s - \vec{K}_i$, is perpendicular to the director $\hat{n}$ ($\vec{q} = \vec{q}_\perp$). In this case, splay and twist fluctuations contribute simultaneously to the scattering. The measured light intensity (divided by the incident light intensity I_o) for normal incidence is given by [32]:

$$\frac{I_{\mathrm{ST}}(\theta_{\mathrm{l}})}{I_{\mathrm{o}}} = (\Delta\varepsilon')^2(\pi\lambda^{-2})^2\Omega dAk_{\mathrm{B}}T\left[\frac{G_1(\theta_{\mathrm{l}})}{K_{11}q_{\perp}^2(\theta_{\mathrm{l}})} + \frac{G_2(\theta_{\mathrm{l}})}{K_{22}q_{\perp}^2(\theta_{\mathrm{l}})}\right], \tag{6}$$

where θ_{l} is scattering angle in the laboratory, $\Delta\varepsilon'$ is optical dielectric anisotropy defined as $\Delta\varepsilon' = n_e^2 - n_o^2$, λ is the wavelength of light, T is the absolute temperature, Ω is collection solid angle, A is the cross-sectional area of the illuminated sample volume, and d is the sample thickness. $G_1(\theta_{\mathrm{l}})$ and $G_2(\theta_{\mathrm{l}})$ are geometrical scattering factors dependent on n_o, n_e and θ_{l}. By choosing the scattering angle to be the so-called "magic angle", $\theta_{\mathrm{m}} = \sin^{-1}\left(n_o\sqrt{1-\frac{n_o^2}{n_e^2}}\right)$, the contribution of twist fluctuation mode to the total intensity disappears, so that $I_{\mathrm{S}}(\theta_{\mathrm{m}}) \propto \frac{G_1(\theta_{\mathrm{m}})}{K_{11}q_{\perp}^2(\theta_{\mathrm{m}})}$. In this case, we can extract the elastic constant K_{11}. The fitted n_o and n_e values of CB7CB at the same wavelength as used for DLS were used to determine θ_{m} at each temperature. The calculated values of θ_{m} vary over $33° - 40°$ within the N range. For the 8OCB control sample, we used literature values of the refractive indices to obtain θ_{m} [33].

In geometry "2" ("twist-bend" geometry), where $\hat{\mathrm{n}}$ lies in scattering plane, the scattering comes from a combination of the twist-bend normal mode of director fluctuations [32]:

$$\frac{I_{\mathrm{TB}}(\theta_{\mathrm{l}})}{I_{\mathrm{o}}} = (\Delta\varepsilon')^2(\pi\lambda^{-2})^2\Omega dAk_{\mathrm{B}}T\left[\frac{G_3(\theta_{\mathrm{l}})}{K_{33}q_{\parallel}^2(\theta_{\mathrm{l}}) + K_{22}q_{\perp}^2(\theta_{\mathrm{l}})}\right] \tag{7}$$

Here $G_3(\theta_{\mathrm{l}})$ is a geometrical factor appropriate to the twist-bend geometry. At a low experimental scattering angle of $\theta_{\mathrm{l}} = 2°$, the ratio $\frac{q_{\perp}^2(\theta_{\mathrm{l}})}{q_{\parallel}^2(\theta_{\mathrm{l}})} \approx 15$. Since we also know that $K_{22} \gg K_{33}$ for dimer molecules with odd-numbered spacers [21-23], we conclude that $K_{22}q_{\perp}^2(\theta_{\mathrm{l}}) \gg K_{33}q_{\parallel}^2(\theta_{\mathrm{l}})$ for $\theta_{\mathrm{l}} = 2°$, so that, to an excellent approximation, only twist fluctuations contribute in the above expression for the scattered intensity. On the other hand, when $\theta_{\mathrm{l}} = \theta_{\mathrm{m}}$, one finds that $q_{\perp}^2(\theta_{\mathrm{m}}) = 0$ [32], and in this case only bend fluctuations are probed. Thus, by switching from very small θ_{l} to $\theta_{\mathrm{l}} = \theta_{\mathrm{m}}$, we can selectively probe the elastic constants K_{22} and K_{33}.

As mentioned previously, in order to obtain the absolute values of the moduli, pure splay, bend, or twist scattering from CB7CB must be calibrated against the corresponding scattering from 8OCB. Literature values of optical parameters ($n_{e,8\mathrm{OCB}} = 1.65$, $n_{o,8\mathrm{OCB}} = 1.50$) [31] and elastic constants ($K_{11,8\mathrm{OCB}} = 5.5$ pN, $K_{22,8\mathrm{OCB}} = 2.9$ pN and $K_{33,8\mathrm{OCB}} = 6.05$ pN) [29,30] at $T - T_{\mathrm{NI}} = -6$ °C were used in order to calculate intensity ratios between the 8OCB and CB7CB samples at fixed temperature ($T - T_{\mathrm{NI}} = -9$ °C). That enables a straightforward calculation of the elastic constants of CB7CB.

DLS also provides information on the orientational viscosities. At optical frequencies the director fluctuation modes are overdamped, and the standard expression for the homodyne intensity correlation function is [34],

$$\langle I(0,\theta_1) I(\tau,\theta_1)\rangle = I(\theta_1)^2 \left[1 + e^{-2\Gamma(\theta_1)\tau}\right] \tag{8}$$

where $\Gamma(\theta_1)$ is the relaxation rate of the fluctuations, and τ is the correlation delay time. Fits of the correlation data to this expression give the relaxation rates for the two director normal modes [32]:

$$\Gamma_\alpha(\theta_1) = \frac{(K_{33} q_{\|}^2 + K_\alpha q_\perp^2)}{\eta_\alpha(\vec{q})},\ \alpha = 1,2 \tag{9}$$

The viscosities $\eta_\alpha(\vec{q})$ are combinations of the Leslie and Miesowicz viscosities of the nematic. From the scattering geometries described above, values of the elastic moduli, and the fitted relaxation rates, we calculate the orientational viscosities for pure bend and splay scattering geometries as [34]:

$$\eta_{\mathrm{splay}} = \frac{K_{11} q_\perp^2}{\Gamma_1(\theta_{\mathrm{m}})} = \eta_1(q_\perp) = \gamma_1 - \frac{\alpha_3^2}{\eta_b} \tag{10}$$

$$\eta_{\mathrm{bend}} = \frac{K_{33} q_{\|}^2}{\Gamma_2(\theta_{\mathrm{m}})} = \eta_2(q_{\|}) = \gamma_1 - \frac{\alpha_2^2}{\eta_c} \tag{11}$$

where $\gamma_1, \alpha_2, \alpha_3, \eta_b, \eta_c$ are fundamental viscosities of the nematic fluid discussed in standard texts [32].

The corresponding orientational diffusivities, D, are found using the following relationships [32]:

$$D_{\text{splay}} = \frac{K_{11}}{\eta_{\text{splay}}} \tag{12}$$

$$D_{\text{bend}} = \frac{K_{33}}{\eta_{\text{bend}}} \tag{13}$$

In the case of the twist-bend mode (geometry "2") for small scattering angle $\theta_1 \approx 2°$ and $\frac{q_\perp^2}{q_\parallel^2} \approx 15$, the orientational viscosity becomes [32]

$$\eta_{\text{twist-bend}} = \frac{K_{22} q_\perp^2}{\Gamma_2(\theta_1 = 2°)} = \eta_2 (q_\perp^2 \approx 15 q_\parallel^2) \approx \gamma_1 - \frac{\alpha_2^2}{\eta_a} \frac{q_\parallel^2}{q_\perp^2} \approx \gamma_1 - \frac{\alpha_2^2}{15\eta_a} \tag{14}$$

In contrast to the situation with the elastic constants, the orientational viscosity $\eta_{\text{twist-bend}}$ cannot be reasonably approximated by the pure twist contribution ($\eta_{\text{twist}} = \gamma_1$), since the value of $\frac{\alpha_2^2}{\eta_a}$ is typically rather large. For example, using reported values of α_2 and η_a for the standard monomeric calamitic 5CB [35], we have $\frac{\alpha_2^2}{\eta_a} = 0.22 \text{ Pa} \cdot \text{s}$ at a temperature 10°C below isotropic-nematic transition, which means that in 5CB the last term in Eq. (14) is 16% of the reported value of $\gamma_1 = 0.08 \text{ Pa} \cdot \text{s}$. Thus, in the following section we report the orientational viscosity in Eq. (14) and the corresponding diffusivity

$$D_{\text{twist-bend}} = \frac{K_{22}}{\eta_{\text{twist-bend}}} \tag{15}$$

III. RESULTS

A. Refractive indices and birefringence

The measurements of the principal refractive indices and the birefringence at $\lambda = 633$ nm are presented in Fig.6.

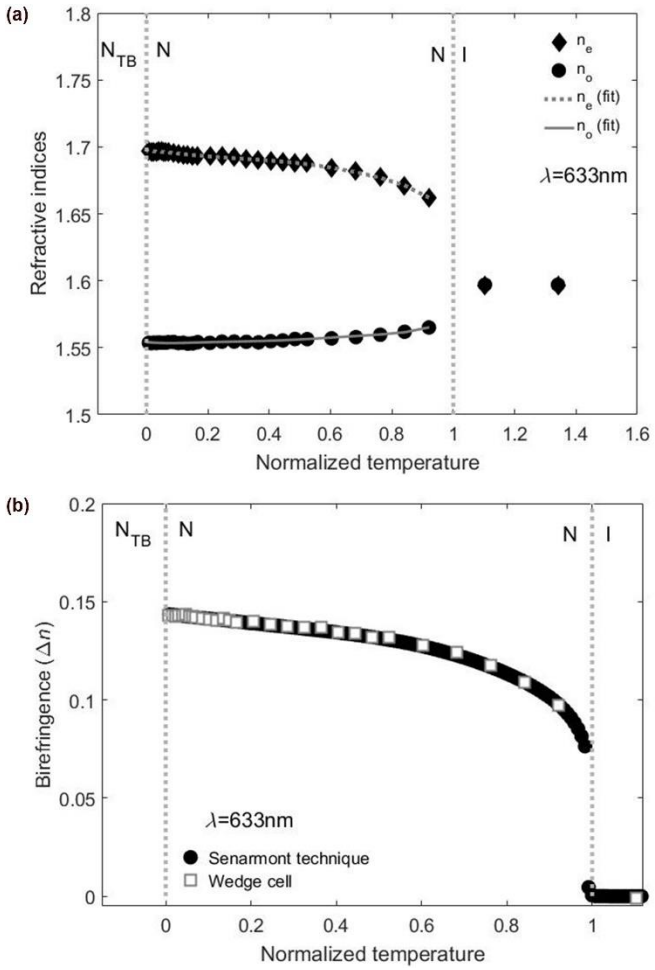

FIG 6. (a) Refractive indices of CB7CB ($\lambda = 633$ nm); filled symbols represent the data acquired using a planar wedge cell; dotted and solid lines represent the fitted values of n_o and n_e respectively; (b) Δn measured at $\lambda = 633$ nm using Senarmont technique (circles), planar wedge cell (squares).

The birefringence is positive and increases monotonically with decreasing temperature through the nematic phase down to the N-N_{TB} transition.

B. Dielectric and diamagnetic properties

Both components of dielectric permittivity ($\varepsilon_{\parallel}$ and $\varepsilon_{\perp}$) are presented in Fig.7(a) as functions of temperature. Fig.7(b) shows that, upon cooling from the I phase, $\Delta\varepsilon$ first significantly

increases and then monotonously decreases. Changing the frequency in the range $f = 5 - 60$ kHz did not significantly affect the temperature dependent behavior of the dielectric constants.

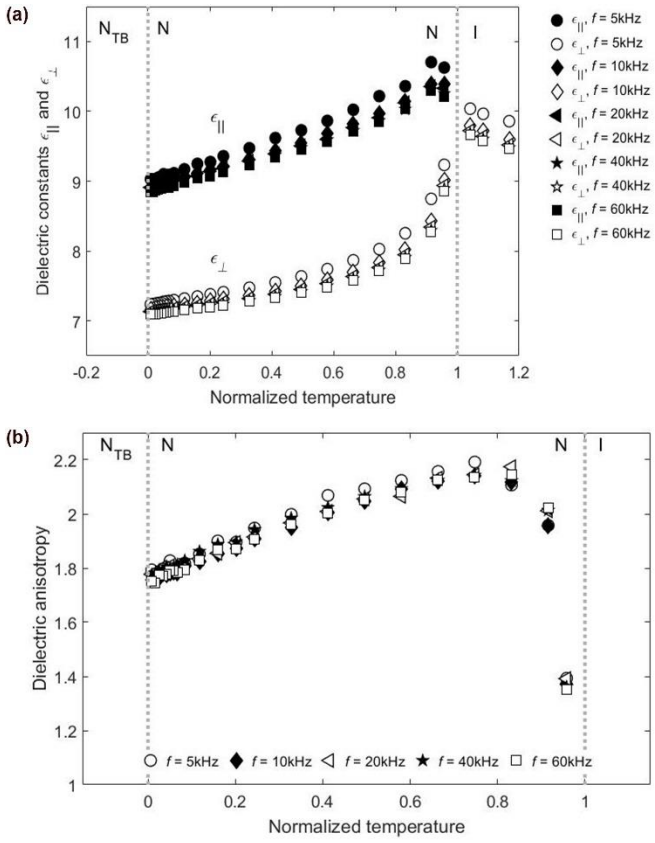

FIG 7. (a) Parallel and perpendicular components of temperature dependent dielectric constants and (b) $\Delta\varepsilon$ measured at $f = 5, 10, 20, 40$ and 60 kHz using a planar cell ($d = 18.9$ μm).

The diamagnetic anisotropy presented in Fig.8(a) has a sharp increase near the I-N transition. It grows with decreasing temperature and saturates towards the N-N_{TB} transition. The data were fitted with a Haller's rule [36] of the form

$$\Delta\chi = \chi_o \left(1 - \frac{T}{T^*}\right)^{\nu} \tag{16}$$

where $\chi_o = 2.1493 \times 10^{-6}$, $T^* = 384.75$ and $\nu = 0.10953$ are the fitting parameters. The scalar nematic order parameter S was calculated using the relationship $S = \frac{\Delta\chi(T)}{\chi_o}$, and is presented in Fig.8(b).

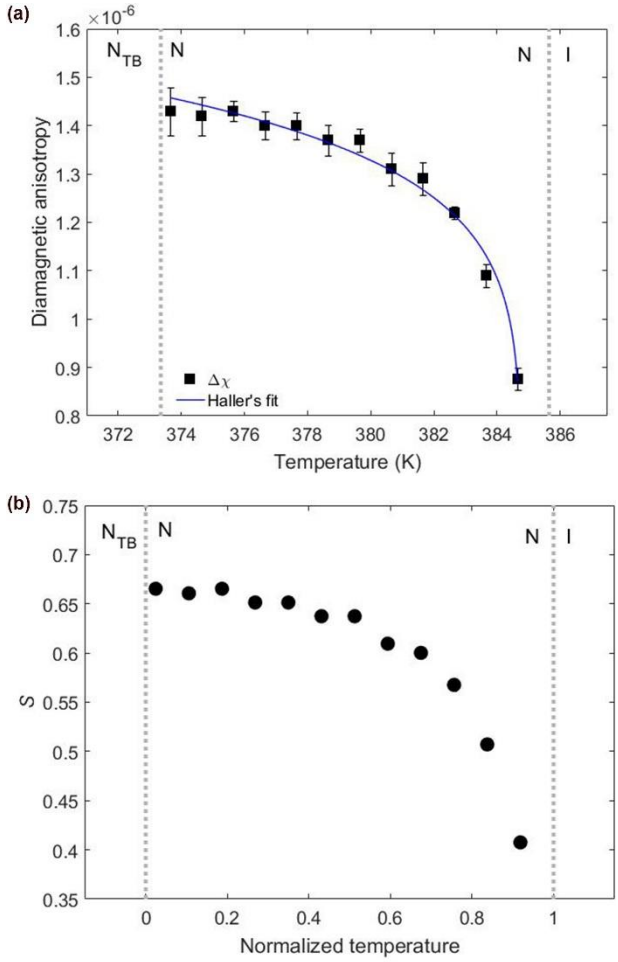

FIG 8. (Color online) (a) Temperature dependence of $\Delta\chi$ fitted with Haller's rule and (b) orientational order parameter.

B. Elastic constants

We performed direct measurements of all three elastic constants of CB7CB by the methods described above. The geometries described in Sec.II for DLS measurements allowed us to isolate the fluctuations related to splay, twist and bend. The independently calculated values of K_{11}, K_{22} and K_{33} from the intensity measurements are presented in Fig. 9(a). The Frederiks transition method was also employed to further assure the validity of DLS results. The results of capacitance measurements at $f = 60$ kHz yielding K_{11} are presented in Fig. 9(a). On cooling, K_{11} weakly

increases in the entire N range. There is also a slight increase in K_{22}, which is more prominent near the N-N_{TB} transition. The most striking behavior, however, is seen in the development of K_{33} as the temperature approaches the N_{TB} phase, Fig. 9(b). On cooling through higher temperatures in the N phase K_{33} increases slightly; however, on further cooling the value dramatically decreases approaching about 0.4 pN, after which there is a sharp growth near the N-N_{TB} transition. The temperature-dependent elastic constant ratios, $\frac{K_{11}}{K_{22}}$, $\frac{K_{33}}{K_{22}}$ and $\frac{K_{11}}{K_{33}}$, are presented in Fig. 10.

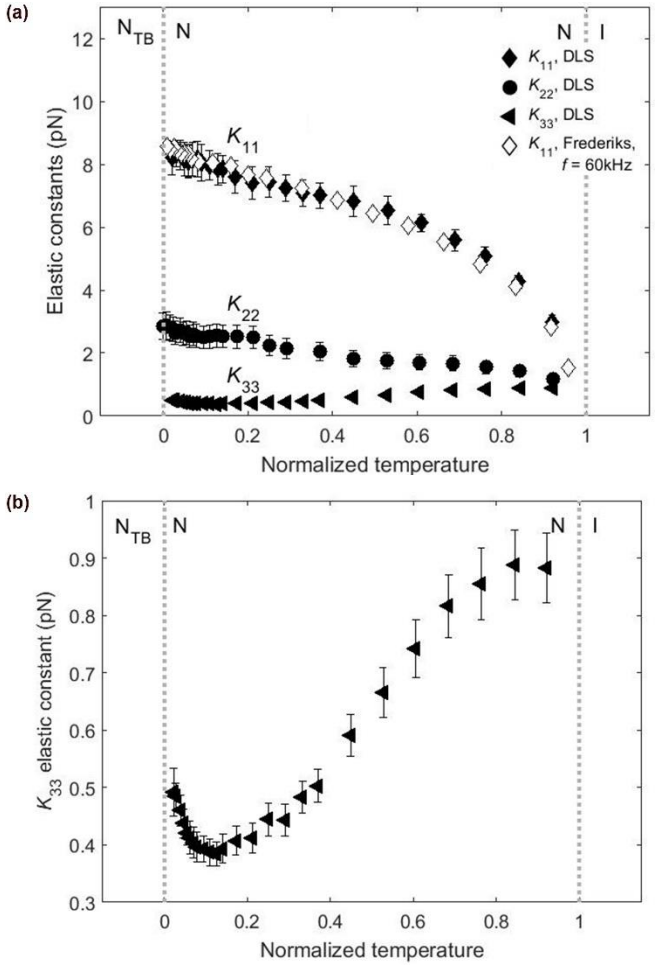

FIG 9. (a) K_{11}, K_{22} and K_{33} measurements acquired using DLS measurements and K_{11} data using capacitance method at $f = 60$ kHz; (b) temperature behavior of K_{33} (DLS method).

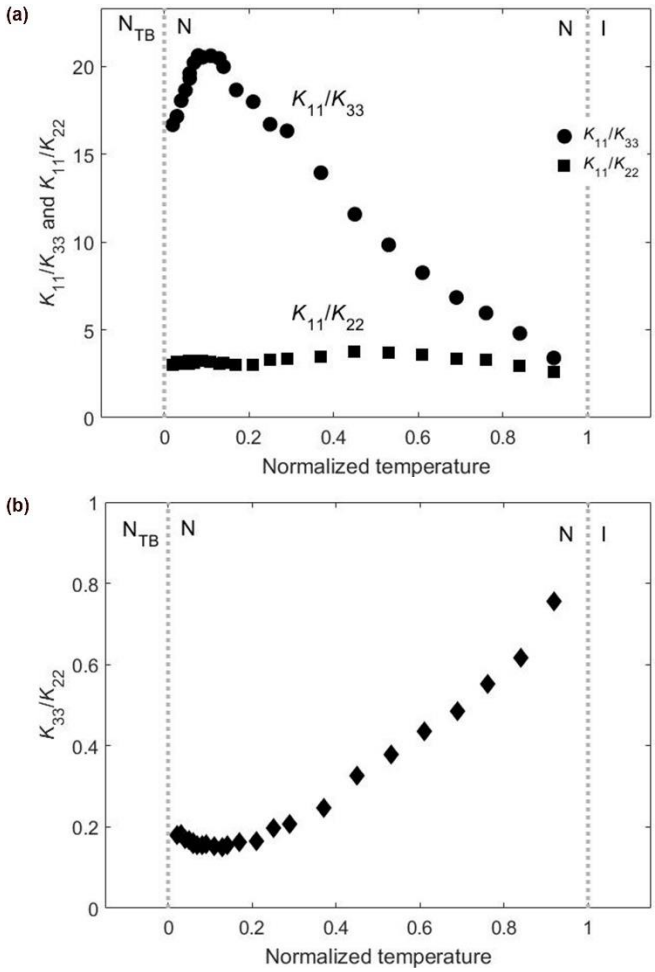

FIG 10. Ratio of elastic constants (a) $\frac{K_{11}}{K_{33}}$ and $\frac{K_{11}}{K_{22}}$, (b) $\frac{K_{33}}{K_{22}}$ from DLS data.

The temperature dependence of the three orientational viscosities, η_{splay}, η_{bend}, and $\eta_{\text{twist-bend}}$ are displayed in Fig. 11; they tend to increase upon cooling, especially on approaching the N_{TB} phase. The corresponding diffusivities defined in Eqs. (12,13,15) are presented in Fig.12. As temperature is lowered from the I phase, $D_{\text{twist-bend}}$ remains practically constant, D_{splay} gradually decreases, and D_{bend} sharply decreases and levels off near the N-N_{TB} transition.

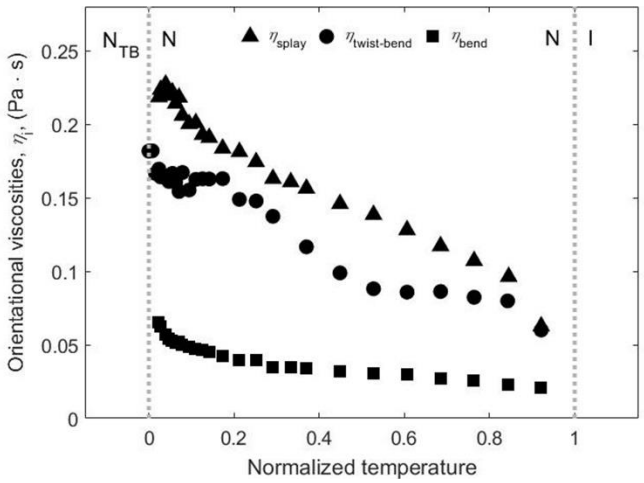

FIG 11. Temperature dependence of orientational viscosities.

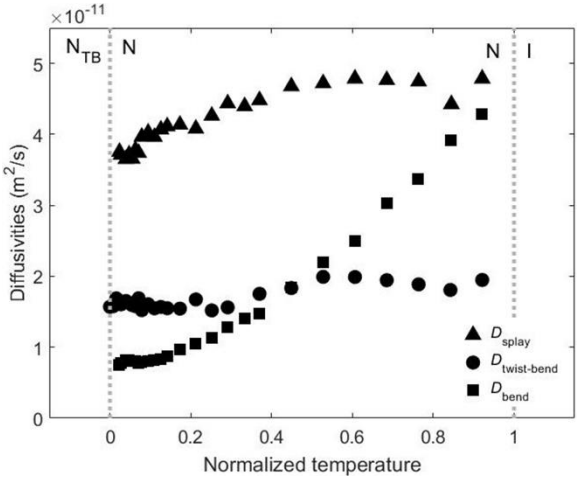

FIG 12. Temperature dependence of orientational diffusivities.

IV. DISCUSSION

The temperature dependence of the refractive indices and birefringence of CB7CB in the N phase is similar to that of ordinary calamatic liquid crystals such as 5CB as well as bent-core liquid crystals [33,35,37-43]. On cooling, the extraordinary refractive index increases and the ordinary index decreases. The birefringence Δn (Fig.6b) is positive and grows with increasing orientational order. The temperature dependence of Δn measured by us at 633 nm is in good agreement with the data by Meyer et al at $\lambda = 546$ nm [44] and Tuchband et al at $\lambda = 656.3$ nm [45].

The measured temperature dependency of dielectric anisotropy $\Delta\varepsilon$ differs from that of Δn . Upon cooling, Δn increases monotonously (Fig.6b), while $\Delta\varepsilon$ first slightly increases near the clearing point, then it decreases (Fig. 7b). The difference between $\Delta\varepsilon(T)$ and $\Delta n(T)$ should not come as a surprise, as at optical frequencies, the electrical polarizability of nematics (and thus Δn) reflects electronic and atomic polarizabilities [46,47], while the value of $\Delta\varepsilon$ at lower frequencies is also influenced by the orientational polarizability. The difference in contributing mechanisms to $\Delta\varepsilon$ and Δn is well known in the studies of rod-like mesogens, see, for example, Refs. [47,48].

The tendency of the perpendicular component of permittivity to decrease on cooling is similar to that for monomeric liquid crystals with $\Delta\varepsilon > 0$ [1]. However, the parallel component of the dielectric permittivity does not behave as in a typical calamitic nematic with $\Delta\varepsilon > 0$, where $\varepsilon_{\parallel}$ is expected to increase on cooling. In CB7CB, $\varepsilon_{\parallel}$ increases slightly just below the I-N transition, but upon further cooling it rolls over and begins to decrease. As seen in Fig. 7, the decrease in $\varepsilon_{\parallel}$ leads to a decline in $\Delta\varepsilon$. Our experimental results are in good agreement with other dielectric studies of CB7CB and its longer homologues [1,15,16,18,23,49-52] and can be qualitatively explained as follows.

In CB7CB, the molecular net dipole moment is determined mostly by the orientation of two cyanobiphenyl groups [1,16,51]. The flexible dimers respond to changes in temperature by modifying their conformations [1,53-56]. Theoretical models of flexible dimers suggest that there are two main populations of conformers, extended and hairpin-like, that vary in the angle between the two terminal cyanobiphenyl units [1]. This angle is about $120°$ for the extended conformers and $30°$ for the hairpin conformers. While the hairpin conformers might contribute substantially to the overall dielectric permittivity near the clearing point, their population should diminish as the temperature is lowered and the packing density increases. At the same time, the population of extended conformers should be growing as the order parameter increases upon cooling [1]. The extended conformers with the angle between two terminal groups above $90°$ should have a vanishing longitudinal dipole moment [16,51]. The effect of increased number of the extended conformers might contribute to the observed decrease of $\varepsilon_{\parallel}$ upon cooling in Fig.7a. Besides the orientation of the dipole groups, their relative position might also contribute to the unusual temperature dependence of permittivity. A non-monotonous temperature dependence of $\Delta\varepsilon$ is known for the nematics formed by rod-like and bent-core molecules near the transition of the N

phase to the smectic-A (SmA) phase [38,47,48]. In SmA, the molecules are arranged in layers, with their long axes being perpendicular to these layers. The spacing between the molecules within SmA layers is shorter than the distance between different planes. This packing feature enhances antiparallel dipole correlations within the layers, decreasing the effective longitudinal dipole moment and thus decreasing $\varepsilon_{\|}$ and $\Delta\varepsilon$ [47,48]. Although the nematic phases of CB7CB do not show smectic modulations of density, enhancement of antiparallel correlations of the dipole moments located at the neighboring molecules might also contribute to the observed decrease of $\varepsilon_{\|}$ and $\Delta\varepsilon$.

The diamagnetic anisotropy of CB7CB is positive, and, as expected, the temperature dependence is similar to that of the birefringence. The values of $\Delta\chi$ saturate near the N-N_{TB} transition. The extrapolated values of the orientational order parameter using Haller's fit show that the scalar order parameter S varies between 0.41 and 0.67, which is consistent with the reported values [44,57].

Figure 11 shows the temperature dependent orientational viscosities that obey a relationship $\eta_{\text{twist-bend}} \approx \eta_{\text{splay}} > \eta_{\text{bend}}$ in the entire nematic range. As already discussed, see Eq. (14), the value of $\eta_{\text{twist-bend}}$ cannot be approximated by the pure rotational viscosity γ_1, since one expects $\eta_{\text{twist-bend}} > \gamma_1$. The value of η_{splay} is about 2 times larger than that in 5CB, while η_{bend} is 10-20% smaller than in 5CB [35]. The increase of η_{splay} in CB7CB as compared to 5CB can be associated with the increase of the molecular length [35]. One expects $\eta_{\text{splay}} > \eta_{\text{bend}}$ for conventional rod-like mesogens [58]. For rigid bent-core molecules, Majumdar et al reported $\eta_{\text{bend}} \approx \eta_{splay}$, with bend viscosity being slightly, by about 10% higher than the splay viscosity [24]. The relative smallness of η_{bend} observed in our studies of CB7CB is apparently caused by the tendency of odd-numbered dimers to adopt bent conformations.

The main focus of this report was to determine the elastic constants in the most accurate and complete fashion. In order to achieve this goal, we used direct measurements by two independent techniques, DLS and Frederiks transition. The elastic moduli obtained in our work and the results of similar studies by other groups for CB7CB are presented in Table I and discussed below. Since the literature values of the nematic range of CB7CB vary, we normalized the temperature (T_{norm}) of the N phase, where T_{norm}=0 and T_{norm}=1 represent N-N_{TB} and I-N transitions

respectively. Table I presents the data for two normalized temperature points $T_{\text{norm}} \approx 0.1$ and ≈ 0.2. In our set-up for CB7CB, these temperatures corresponds to ~102.3 ˚C and ~103.6 ˚C respectively. The literature values of K_{11}, K_{22}, K_{33} for CB7CB were taken from the supplementary material in Ref. [15] as well as from the figures in Refs. [16,18,19]. Experimental errors presented in Table I were calculated by error propagation method for DLS data and by measuring the symbol size in plots presented in Refs. [15,16,18,19].

Table I. Elastic constants and their ratios of CB7CB dimer, 8OCB calamitic mesogen (I-N-SmA transitions), bent-core mesogens 12-F (I-N-SmA) and A131 (I-N-SmC) at $T_{\text{norm}} \approx 0.1$ and 0.2. The normalized temperature equals 1 at the I-N transition point and 0 at the transition point from N to the lower-temperature phase.

Material	T_{norm}	K_{11} (pN)	K_{22} (pN)	K_{33} (pN)	$\frac{K_{11}}{K_{22}}$	$\frac{K_{11}}{K_{33}}$	Reference
CB7CB	0.1	8.0 ± 0.5	2.5 ± 0.4	0.39 ±0.02	3.2	21	DLS (this work)
CB7CB	0.1	7.2 ± 0.3	5.2 ± 0.5	0.3 ± 0.1	1.4	24	Ref. [15]
CB7CB	0.1	7.6 ± 0.2	-	0.6 ± 0.2	-	13	Ref. [16]
CB7CB	0.1	7.0 ± 0.2	-	3.8 ± 0.3	-	1.8	Ref. [18]
CB7CB	0.1	7.6 ± 0.3	-	0.5 ± 0.3	-	15	Ref. [19]
CB7CB	0.2	7.4 ± 0.5	2.4 ± 0.4	0.41 ± 0.03	3.1	18	DLS (this work)
CB7CB	0.2	6.9 ± 0.3	4.9 ± 0.3	0.3 ± 0.1	1.4	23	Ref. [15]
CB7CB	0.2	7.2 ± 0.2	-	0.6 ± 0.2	-	12	Ref. [16]
CB7CB	0.2	6.8 ± 0.2	-	3.7 ± 0.3	-	1.8	Ref. [18]
CB7CB	0.2	7.1 ±0.3	-	0.6 ± 0.3	-	12	Ref. [19]
8OCB	0.1	7.3 ± 0.1	4.0 ± 0.1	13.1 ±0.1	1.8	0.56	Ref. [30]
8OCB	0.2	6.8 ± 0.1	3.5 ± 0.1	9.5 ± 0.1	1.9	0.72	Ref. [30]
12-F	0.1	6.7 ± 0.5	-	9.4 ± 0.4	-	0.71	Ref.[38]
12-F	0.2	6.2 ± 0.5	-	5.9 ± 0.3	-	1.1	Ref.[38]
A131	0.1	15.4 ± 0.3	-	11.6 ± 0.3	-	1.3	Ref. [59]
A131	0.2	13.9 ± 0.3	-	6.7 ± 0.3	-	2.1	Ref. [59]

Splay. The splay modulus data measured by our two methods agree with each other within the error bars, Fig. 9a. Upon cooling, K_{11} grows monotonously, and obeys the relationship $K_{11} > K_{22}, K_{33}$ throughout the entire N range. The K_{11} values are in a reasonable agreement with the literature data obtained by measuring capacitance of cells experiencing the splay Frederiks transition [15,16,18,19], Table I. The major source of the error in the DLS measurements is the

variation of the measured light intensity values. We minimized that error by measuring the light intensity of each data point by two independent channels for ten minutes.

Twist. The dependence $K_{22}(T)$ measured by DLS shows a typical increase as the temperature is lowered. The rate of this increase becomes higher near the N-N_{TB} phase transition, within about 1.2˚C of the transition point. The absolute values, however, are lower than the values reported for K_{22} in Ref. [15], by a factor of ~ 2 near the N-N_{TB} transition. The authors in Ref. [15] used the electric Frederiks transition in a twisted nematic (TN) cell and in a planar cell with in-plane switching (IPS). According to Ref. [15], the obtained values of K_{22} are not accurate because of difficulties in determining the threshold voltage V_{th} in the TN cells and because of field inhomogeneity in the IPS cells. The ratio $\frac{K_{11}}{K_{22}}$ measured in our work is consistently higher than 2.5 in the entire N range of CB7CB, while Ref. [15] reports that on average $\frac{K_{11}}{K_{22}} \approx 1.4$. Note here that the twist-bend phase has been predicted to be stable only when $\frac{K_{11}}{K_{22}} > 2$, as opposed to the splay-bend case in which one expects $\frac{K_{11}}{K_{22}} < 2$ [6,60].

Bend. The most striking temperature dependence is observed for K_{33}. Our DLS data show an overall decrease of K_{33} upon cooling, down to ≈ 0.4 pN near the N-N_{TB} transition, after which K_{33} grows within 1.5˚C interval just before the transition. A similar pretransitional slight increase of K_{33} was already observed for CB7CB and other dimeric liquid crystals [16,19,21-23,51], with the exception of Ref. [18] which reported K_{33} monotonously increasing as the temperature is lowered. In Refs. [15,16,18,19] K_{33} was determined by using the splay Frederiks transition and measuring the cell's response well above the threshold voltage at which pure splay gives rise to mixed splay-bend; extrapolation to infinite fields yields K_{33}. When $K_{33} \ll K_{11}$, this extrapolation might be less accurate than in the conventional case of $K_{33} > K_{11}$. Furthermore, as the electric field increases above threshold, director deformations give rise to flexoelectric polarization that renormalizes the extrapolated value of the elastic constants. In particular, Brown and Mottram [61]

demonstrated that in the conventional nematic E7, the extrapolated values of K_{33} obtained from the splay Frederiks effect in a planar cell are significantly influenced by this flexoeffect. In the case of CB7CB, the flexoelectric effect can be significant, see, for example, [62,63]. Thus the extrapolation technique should be supplemented by an independent analysis of how the flexoelectric effect can influence the extrapolated K_{33} .Thus far, only our DLS experiments provide a direct measurement of K_{33} . The data show that the splay-bend anisotropy of the elastic constants in CB7CB is huge, $\frac{K_{11}}{K_{33}} \sim 21$, which implies that the one-constant approximation ($K_{11} = K_{22} = K_{33}$) often used in theory will not be accurate for CB7CB.

Table I also compares the elastic moduli of CB7CB to those of other nematics, formed by conventional rod-like and rigid bent-core molecules with underlying smectic phases. Again, we use normalized temperature to make the comparison, where T_{norm}=0 represents N-SmA/SmC transition. 8OCB is a calamitic liquid crystal which exhibits N-SmA transition [30]. Bent-core compound (4*'*-fluoro phenyl azo) phenyl-4-yl 3-[*N*-(4*'*-*n*-dodecyloxy 2-hydroxybenzylidene)amino]-2-methyl benzoate abbreviated as 12-F, exhibits SmA phase [38], while the second bent-core material, 4-[(4-dodecylphenyl)diazenyl] phenyl 2-methyl-3-[4-(4-octylbenzoyloxy) benzyledeneamino] benzoate, abbreviated as A131, exhibits SmC phase [59].

Nematic phases of 8OCB, F-12 and A131, listed in Table I, all exhibit a substantional pretransitional increase of K_{33} when temperature is cooled down from $T_{\text{norm}} = 0.2$ to $T_{\text{norm}} = 0.1$. The effect is usually explained by the proximity of the smectic phase in which the condition of layers equidistance is incompatible with the director bends and twists; above the transition, in the N phase, formation of cybotactic clusters with periodic layer spacing makes twist and bend elastic constants relatively large [30,33,38,59]. Even though the N_{TB} phase of CB7CB does not exhibit periodic mass density modulation, the periodic director structure limits twist and bend [22]. Thus, the mechanism responsible for the observed pretransitional increase of K_{22} and K_{33} near N-N_{TB} phase transition in CB7CB, Fig.9, may be analogous to that of other materials near the N-SmA/SmC phase transitions, where K_{22} and K_{33} diverge.

The results presented in this work and in Refs. [21-23] demonstrate that the typical elastic constants relationship for the N phase of dimers exhibiting the N_{TB} phase is of the type $K_{33} < K_{22} < K_{11}$. For rod-like calamitic nematics such as 8OCB, Table I, the relationship is

$K_{22} < K_{11} < K_{33}$ [22,30,64,65]. In the case of bent-core nematics, however, the elastic constant relationship is not universal, and it is largely dependent on the bend angle [43,66]. Few reports show that $K_{33} > K_{11}$ [38,43,67]. There are also observations of an anomalous temperature behavior, similar to dimers, with $K_{33} < K_{11}$ [24,38,42,59,68]. The bent shape of the rigid bent-core molecules might explain the anomalously small K_{33} [59]. The reduction of the bend elastic constant by the molecular curvature has already been predicted by Gruler and Helfrich [69,70].

V. CONCLUSION

In this report, we experimentally determined the temperature-dependent optical, dielectric, diamagnetic and elastic and viscous material properties of the most studied odd methylene-linked dimer, CB7CB, in its nematic phase. We determined that on cooling, the refractive indices behave much like the regular calamatic liquid crystals such as 5CB. The dielectric measurements reveal that the parallel component of dielectric permittivity decreases on approach to the N-N_{TB} transition after an initial increase below the isotropic phase, while the perpendicular component decreases monotonically. The resultant dielectric anisotropy has a sharp increase below the clearing temperature, but then rolls over and gradually decreases on approaching the N-N_{TB} transition. These results are consistent with the dimers adopting a more bent (less extended) average conformation as the N-N_{TB} transition is approached.

We also reported the first independent temperature dependent measurements of all three elastic constants for CB7CB. In our study we employed direct measurements of all three elastic constants with very small temperature steps near N-N_{TB} phase transition. We show that the relationship $K_{11} > K_{22} > K_{33}$ holds true in the entire nematic range, with $\frac{K_{11}}{K_{22}} > 2$ as predicted by the theory for a system that exhibits the N_{TB} phase [6,60]. K_{11} increases monotonously; K_{22} also increases gradually but has a more prominent pretransitional increase close to the N-N_{TB} phase transition. The temperature dependence of K_{33} is the most dramatic – on cooling from the I-N transition it decreases to an unusually low value ≈ 0.38 pN and then experiences pretransitional increase near the N-N_{TB} transition. The pretransitional increase of both K_{22} and K_{33} might be

explained by formation of clusters with periodic twist-bend modulation of the director close to N_{TB} phase transition. These clusters lead to an increase of K_{22} and K_{33} since the equidistance of pseudolayers hinders twist and bend deformations of the director. A similar pretransitional increase of K_{22} and K_{33} is well documented near the nematic-to-smectic A phase transition [30,71,72]. The ratio $\frac{K_{33}}{K_{22}}$ that controls the field-tunable range of the heliconical structure [73] is less than 1 in the entire N range, thus making CB7CB a good candidate for preparation of heliconical cholesterics with a tunable pitch.

Finally, the measured values of all three orientational viscosities increase on cooling, showing steeper slopes near the N-N_{TB} phase transition. The bend orientational diffusivity sharply decreases on cooling from T_{NI} and saturates near $T_{N_{TB}}$. The splay diffusivity decreases smoothly, whereas, on average, the twist diffusivity remains constant throughout the nematic range.

Acknowledgments

The work was supported by NSF grants DMR-1410378 and DMR-1307674. The authors acknowledge R. Stayshich for purifying 8OCB.

G.B. and Z.P. contributed equally to this work.

References

[1] M. Cestari *et al.*, Phys Rev E **84**, 031704 (2011).
[2] D. Chen *et al.*, P Natl Acad Sci USA **110**, 15931 (2013).
[3] V. Borshch *et al.*, Nat Commun **4**, 2635 (2013).
[4] C. Zhu *et al.*, Phys Rev Lett **116**, 147803 (2016).
[5] R. B. Meyer, *Structural problems in liquid crystal physics* (Gordon and Breach, New York, 1976), Les Houches Summer School in Theoretical Physics, 1973. Molecular Fluids.
[6] I. Dozov, EPL (Europhysics Letters) **56**, 247 (2001).
[7] R. Memmer, Liquid Crystals **29**, 483 (2002).
[8] J. Xiang, S. V. Shiyanovskii, C. T. Imrie, and O. D. Lavrentovich, Phys Rev Lett **112**, 217801 (2014).
[9] J. Xiang, Y. N. Li, Q. Li, D. A. Paterson, J. M. D. Storey, C. T. Imrie, and O. D. Lavrentovich, Adv Mater **27**, 3014 (2015).
[10] S. M. Salili *et al.*, Phys Rev E **94**, 042705 (2016).
[11] R. B. Meyer, Appl Phys Lett **12**, 281 (1968).
[12] P. G. d. Gennes, Solid State Commun **6**, 163 (1968).
[13] A. B. Harris, R. D. Kamien, and T. C. Lubensky, Rev Mod Phys **71**, 1745 (1999).

[14] J. Xiang, A. Varanytsia, F. Minkowski, D. A. Paterson, J. M. D. Storey, C. T. Imrie, O. D. Lavrentovich, and P. Palffy-Muhoray, P Natl Acad Sci USA **113**, 12925 (2016).
[15] C.-J. Yun, M. R. Vengatesan, J. K. Vij, and J.-K. Song, Appl Phys Lett **106**, 173102 (2015).
[16] N. Sebastian, B. Robles-Hernandezb, S. Diez-Berart, J. Saludc, G. R. Luckhurst, D. A. Dunmur, D. O. Lopez, and M. R. La Fuente, Liquid Crystals **44**, 177 (2017).
[17] S. Parthasarathi, D. S. S. Rao, N. B. Palakurthy, C. V. Yelamaggad, and S. K. Prasad, J Phys Chem B **121**, 896 (2017).
[18] S. Parthasarathi, D. S. S. Rao, N. B. Palakurthy, C. V. Yelamaggad, and S. Krishna Prasad, The Journal of Physical Chemistry B **120**, 5056 (2016).
[19] D. O. Lopez, B. Robles-Hernandez, J. Salud, M. R. de la Fuente, N. Sebastian, S. Diez-Berart, X. Jaen, D. A. Dunmur, and G. R. Luckhurst, Phys Chem Chem Phys **18**, 4394 (2016).
[20] H. J. Deuling, Mol Cryst Liq Cryst **19**, 123 (1972).
[21] K. Adlem *et al.*, Phys Rev E **88**, 022503 (2013).
[22] G. Cukrov, Y. Mosaddeghian Golestani, J. Xiang, Yu. A. Nastishin, Z. Ahmed, C. Welch, G. H. Mehl, and O. D. Lavrentovich, Liquid Crystals **44**, 219 (2017).
[23] N. Sebastian *et al.*, Phys Chem Chem Phys **18**, 19299 (2016).
[24] M. Majumdar, P. Salamon, A. Jakli, J. T. Gleeson, and S. Sprunt, Phys Rev E **83**, 031701 (2011).
[25] S. Zhou, K. Neupane, Yu. A. Nastishin, A. R. Baldwin, S. V. Shiyanovskii, O. D. Lavrentovich, and S. Sprunt, Soft Matter **10**, 6571 (2014).
[26] J. Kędzierski *et al.*, Opto-Electron Rev **18**, 214 (2010).
[27] T. J. Scheffer and J. Nehring, Journal of Applied Physics **48**, 1783 (1977).
[28] Yu. A. Nastishin, R. D. Polak, S. V. Shiyanovskii, V. H. Bodnar, and O. D. Lavrentovich, Journal of Applied Physics **86**, 4199 (1999).
[29] M. J. Bradshaw, E. P. Raynes, J. D. Bunning, and T. E. Faber, J Phys-Paris **46**, 1513 (1985).
[30] N. V. Madhusudana and R. Pratibha, Mol Cryst Liq Cryst **89**, 249 (1982).
[31] B. Kundu, Raman Research Insitute, 2008.
[32] P. G. d. G. a. J. Prost, *The Physics of Liquid Crystals (International Series of Monographs On Physics)* (Oxford: Clarendon Press, 1995), Second edn.
[33] B. Kundu, R. Pratibha, and N. V. Madhusudana, Phys Rev Lett **99**, 247802 (2007).
[34] R. Borsali, D. Y. Yoon, and R. Pecora, J Phys Chem B **102**, 6337 (1998).
[35] M. Cui, Kent State University, 2000.
[36] I. Haller, Progress in Solid-State Chemistry **10**, 103 (1975).
[37] J. Addis, University of Manchester, 2013.
[38] N. Avci, V. Borshch, D. D. Sarkar, R. Deb, G. Venkatesh, T. Turiv, S. V. Shiyanovskii, N. V. S. Rao, and O. D. Lavrentovich, Soft Matter **9**, 1066 (2013).
[39] P. Sathyanarayana, V. S. R. Jampani, M. Skarabot, I. Musevic, K. V. Le, H. Takezoe, and S. Dhara, Phys Rev E **85**, 011702 (2012).
[40] P. Sathyanarayana, B. K. Sadashiva, and S. Dhara, Soft Matter **7**, 8556 (2011).
[41] J. A. Olivares, S. Stojadinovic, T. Dingemans, S. Sprunt, and A. Jakli, Phys Rev E **68**, 041704 (2003).
[42] S. Kaur, J. Addis, C. Greco, A. Ferrarini, V. Gortz, J. W. Goodby, and H. F. Gleeson, Phys Rev E **86**, 041703 (2012).
[43] S. Kaur, L. Tian, H. Liu, C. Greco, A. Ferrarini, J. Seltmann, M. Lehmannd, and H. F. Gleeson, Journal of Materials Chemistry C **1**, 2416 (2013).
[44] C. Meyer, G. R. Luckhurst, and I. Dozov, Journal of Materials Chemistry C **3**, 318 (2015).
[45] M. R. Tuchband *et al.*, ArXiv e-prints **1703**, arXiv:1703.10787 (2017).
[46] L. M. Blinov, V. G. Chigrinov, and L. M. Blinov, *Electrooptic effects in liquid crystal materials* (Springer-Verlag, New York, 1994), Partially ordered systems.
[47] W. H. de Jeu, T. W. Lathouwers, and P. Bordewijk, Phys Rev Lett **32**, 40 (1974).
[48] W. H. de Jeu, W. J. A. Goossens, and P. Bordewijk, The Journal of Chemical Physics **61**, 1985 (1974).

[49] B. Robles-Hernandez, N. Sebastian, J. Salud, S. Diez-Berart, D. A. Dunmur, G. R. Luckhurst, D. O. Lopez, and M. R. de la Fuente, Phys Rev E **93**, 062705 (2016).
[50] N. Sebastian, D. O. Lopez, B. Robles-Hernandez, M. R. de la Fuente, J. Salud, M. A. Perez-Jubindo, D. A. Dunmur, G. R. Luckhurst, and D. J. B. Jackson, Phys Chem Chem Phys **16**, 21391 (2014).
[51] B. Robles-Hernandez *et al.*, Phys Rev E **92**, 062505 (2015).
[52] N. Trbojevic, D. J. Read, and M. Nagaraj, Phys Rev E **96**, 052703 (2017).
[53] A. Ferrarini, G. R. Luckhurst, P. L. Nordio, and S. J. Roskilly, Chem Phys Lett **214**, 409 (1993).
[54] A. Ferrarini, G. R. Luckhurst, P. L. Nordio, and S. J. Roskilly, J Chem Phys **100**, 1460 (1994).
[55] A. Ferrarini, G. R. Luckhurst, and P. L. Nordio, Mol Phys **85**, 131 (1995).
[56] A. Ferrarini, G. R. Luckhurst, P. L. Nordio, and S. J. Roskilly, Liquid Crystals **21**, 373 (1996).
[57] S. Zhou *et al.*, Phys Rev Lett **109**, 037801 (2012).
[58] W. H. d. Jeu, *Physical properties of liquid crystalline materials* (Gordon and Breach, New York, 1980), Liquid crystal monographs, 1.
[59] P. Sathyanarayana, M. Mathew, Q. Li, V. S. S. Sastry, B. Kundu, K. V. Le, H. Takezoe, and S. Dhara, Phys Rev E **81**, 010702 (2010).
[60] S. M. Shamid, S. Dhakal, and J. V. Selinger, Phys Rev E **87**, 052503 (2013).
[61] C. V. Brown and N. J. Mottram, Phys Rev E **68**, 031702 (2003).
[62] A. Varanytsia and L. C. Chien, Sci Rep-Uk **7**, 41333 (2017).
[63] K. S. Krishnamurthy, N. B. Palakurthy, and C. V. Yelamaggad, J Phys Chem B **121**, 5447 (2017).
[64] A. Ferrarini, Liquid Crystals **37**, 811 (2010).
[65] S. Shri, Physics Reports **277**, 283 (1996).
[66] H. F. Gleeson, S. Kaur, V. Gortz, A. Belaissaoui, S. Cowling, and J. W. Goodby, Chemphyschem **15**, 1251 (2014).
[67] P. Salamon, N. Eber, J. Seltmann, M. Lehmann, J. T. Gleeson, S. Sprunt, and A. Jakli, Phys Rev E **85**, 061704 (2012).
[68] P. Tadapatri, U. S. Hiremath, C. V. Yelamaggad, and K. S. Krishnamurthy, J Phys Chem B **114**, 1745 (2010).
[69] H. Gruler, J Chem Phys **61**, 5408 (1974).
[70] W. Helfrich, Mol Cryst Liq Cryst **26**, 1 (1974).
[71] M. Delaye, R. Ribotta, and G. Durand, Phys Rev Lett **31**, 443 (1973).
[72] R. Blinc, I. Muševič, D. Demus, J. Goodby, G. W. Gray, H. W. Spiess, and V. Vill, in *Handbook of Liquid Crystals Set* (Wiley-VCH Verlag GmbH, 1998), pp. 170.
[73] J. Xiang, S. V. Shiyanovskii, Y. N. Li, C. T. Imrie, Q. Li, and O. D. Lavrentovich, Liquid Crystals XVIII **9182**, 91820P (2014).